

Highly-transmitting modes of light in dynamic atmospheric turbulence

David Bachmann,¹ Mathieu Isoard,¹ Vyacheslav Shatokhin,^{1,2}
Giacomo Sorelli,³ Nicolas Treps,³ and Andreas Buchleitner^{1,2}

¹*Physikalisches Institut, Albert-Ludwigs-Universität Freiburg,
Hermann-Herder-Str. 3, D-79104 Freiburg, Germany*

²*EUCOR Centre for Quantum Science and Quantum Computing,
Albert-Ludwigs-Universität Freiburg, Hermann-Herder-Str.3, D-79104 Freiburg, Germany*

³*Laboratoire Kastler Brossel, Sorbonne Université, ENS-Université PSL,
Collège de France, CNRS; 4 place Jussieu, F-75252 Paris, France*

(Dated: April 13, 2022)

We show that instantaneous spatial singular modes of light in a dynamically evolving, turbulent atmosphere offer significantly improved high-fidelity signal transmission as compared to standard encoding bases corrected by adaptive optics. Their enhanced stability in stronger turbulence is associated with a subdiffusive algebraic decay of the transmitted power with evolution time.

Introduction.— Wave transport in random scattering media is ubiquitous in communication, sensing and imaging, from astronomical [1] over mesoscopic [2] to microscopic scales [3]. In all these rather diverse physical settings, the common goal is to faithfully transmit and filter relevant information generated by the sender, probed by the scattering wave, or emitted by some unknown object(s). To achieve an efficient transmission and retrieval of information, it is indispensable to mitigate the random, i.e., uncontrolled modulation of the transmitted signal's phase and intensity profile, with a resolution which is determined by the transmission channel's desired capacity.

For a light field propagating through atmospheric turbulence, a plausible and technologically well advanced strategy to compensate phase errors is offered by *adaptive optics* (AO). In essence, this consists in real-time wavefront shaping either of the input or output signal [1, 4–8]. However, AO cannot compensate for (interference induced) intensity fluctuations upon transmission [9]. Furthermore, a combination of diffraction and refraction in turbulence paired with a finite aperture at the receiver side will ultimately render the communication channel *non-unitary*, i.e., lossy, and thereby further limit the performance of AO.

An alternative strategy which we here propose for signal transmission across a turbulent channel, is to exploit the random medium's intrinsic properties: Wave propagation in static disordered media generically allows for the formation of highly-transmitting spatial modes [10, 11], e.g. *singular modes* obtained by decomposing the channel's transmission matrix. These modes qualify due to their minimal transverse losses as ideal candidates for high-dimensional signal encoding. However, the stability of such highly-transmitting spatial modes is challenged in a *dynamically evolving* medium – here the Earth's atmosphere. Yet, even in this case one can expect that certain robust features of the random medium are inscribed in instantaneous singular modes and lend them

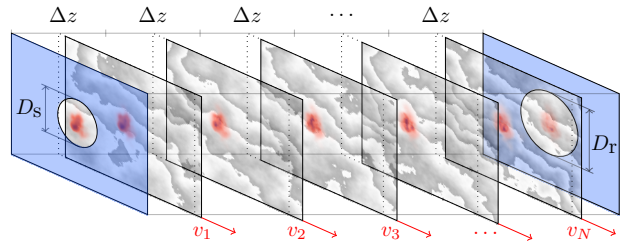


Figure 1. Horizontal transmission channel across a dynamically evolving, turbulent atmosphere: The medium (confined between coaxial circular source and receiver apertures of diameters D_s and D_r , respectively) is represented by a collection of equidistant *phase screens*. The screens' transverse structure and separation Δz are governed by *turbulence strength*, while dynamical aspects are modeled by individual shifting according to wind velocities v_i (red arrows).

persistent stability properties. Our present purpose is to consolidate this expectation, and to quantify the time scales over which highly-transmitting singular modes offer resilient signal transmission with reduced losses.

The model.— We consider a horizontal free-space channel of length L , consisting of a turbulent medium limited by two coaxial circular source and receiver apertures with diameters D_s and D_r , respectively, see Fig. 1. Between the apertures, a scalar monochromatic wave $\psi(\mathbf{r} = x, y, z)$ with wavelength λ obeys the *stochastic parabolic equation* [12]

$$-2ik \frac{\partial \psi(\mathbf{r})}{\partial z} = \Delta_{\perp} \psi(\mathbf{r}) + 2k^2 \delta n(\mathbf{r}, t) \psi(\mathbf{r}), \quad (1)$$

where $k = 2\pi/\lambda$, Δ_{\perp} – the transverse Laplace operator with respect to the propagation axis z – accounts for wave diffraction, and $\delta n(\mathbf{r}, t)$ is the fluctuating part of the refractive index of air, to model the turbulent random scattering potential and its time dependence. The statistical properties of $\delta n(\mathbf{r}, t)$ are governed, according to *Kolmogorov theory* [13], by the refractive in-

dex power spectrum $\Phi_n(\kappa) = 0.033 C_n^2 \kappa^{-11/3}$, with κ the transverse spatial frequency and C_n^2 the refractive index structure parameter which controls the turbulence strength. The *transverse coherence length* of turbulence, which is the typical distance between two points in the transverse plane over which turbulence-induced phase distortions are correlated, is given by the *Fried parameter*, $r_0 = (0.423 k^2 C_n^2 L)^{-3/5}$ [12], and phase fluctuations are governed by Kolmogorov's *phase structure function* $D_\phi(\rho) = 6.88 (\rho/r_0)^{5/3}$ [14], where ρ is the transverse distance. Intensity fluctuations, i.e. the *scintillation* strength [8, 15], are controlled by the Rytov variance, $\sigma_R^2 = 1.229 C_n^2 k^{7/6} L^{11/6}$ [14].

For channel lengths L not exceeding approximately 100 km, the propagation of light between the source and the receiver can be considered instantaneous as compared to the atmospheric coherence time t_c (the typical time scale of dynamical changes of the atmospheric density profile, $\sim 1 \dots 10$ ms) [8]. For fixed times t , a reliable numerical solution of Eq. (1), for a broad range of atmospheric conditions, can be obtained via the *split-step method* [9, 16, 17]. This approach relies on the fact that, for weak scintillation ($\sigma_R^2 \lesssim 1$), the impact of turbulence on the propagating light reduces to phase distortions. We can therefore replace a three-dimensional turbulence channel with arbitrary σ_R^2 by a sequence of equally spaced *phase screens* interconnected by free diffraction in vacuum (cf. Fig. 1). To generate phase screens which obey Kolmogorov statistics, we employ Fourier methods [18] augmented by Zernike polynomials [19].

The combination of phase distortions and free diffraction can be represented as a unitary operator U_{turb} acting on the propagating wave. Furthermore, the effects of source and receiver apertures (see Fig. 1) are captured by projection operators Π_s and Π_r , respectively. Together, this defines the *turbulence operator* T_{turb} of the channel, $T_{\text{turb}} = \Pi_r U_{\text{turb}} \Pi_s$, a propagator (Green's function) which maps modes from the source onto the receiver plane, and is, in general, non-unitary, since light escapes the receiver aperture due to diffraction, turbulence-induced broadening and beam wandering [12].

A *singular value decomposition* (SVD) [10, 20] of T_{turb} yields its orthonormal transmission channels: *Source modes* $v_s(\rho)$ are coupled bijectively to *receiver modes* $u_s(\rho')$, each associated with *singular values* τ_s which quantify the transmitted power per channel. The action of T_{turb} on an input state Ψ thus has the explicit form

$$(T_{\text{turb}} \star \Psi)(\rho') = \sum_{s=0}^{S-1} \sqrt{\tau_s} u_s(\rho') \langle v_s(\rho), \Psi(\rho) \rangle, \quad (2)$$

where \star denotes the convolution, $\rho \in D_s$ and $\rho' \in D_r$ are the transverse position vectors, $\langle \cdot, \cdot \rangle$ stands for the standard scalar product in transverse space, and the number S of singular modes with non-vanishing weight depends on the source and receiver apertures' cross sec-

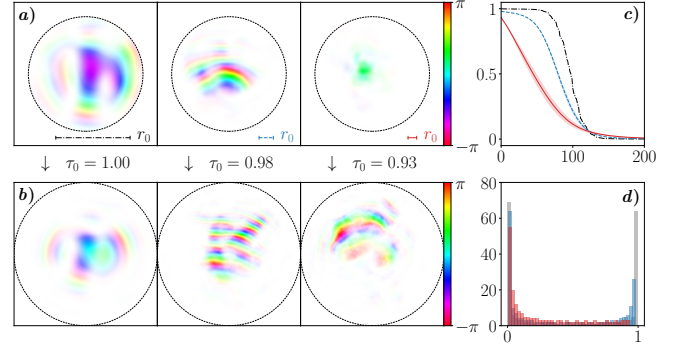


Figure 2. Intensity-weighted transverse phase profiles of the source (a) and receiver (b) singular modes associated with the largest singular value τ_0 of a *single* realization of frozen turbulent medium with Fried parameter $r_0 = 130, 25, 15$ mm, and Rytov variance $\sigma_R^2 = 0.18, 4.16, 6.72$ (left to right) for our channel [21]. (c) distributions of the average singular values $\bar{\tau}_s$ in decreasing order, each obtained by averaging over 500 disorder realizations (error bands give one standard deviation) with same parameters and color code as in (a,b). (d) corresponding histograms.

tions. Practically, the SVD is applied to a matrix representation of the turbulence operator, known as *transmission matrix* $(T_{\text{turb}})_{ij} = \langle \phi_i(\rho'), (T_{\text{turb}} \star \psi_j)(\rho') \rangle$, where $\psi_j(\rho)$ and $\phi_i(\rho')$ are basis modes on the source and receiver side, respectively. For an accurate representation of transmitted fields confined by circular apertures, we choose *Laguerre-Gaussian* (LG) modes at the source side, which also feature convenient diffraction properties [12]. To resolve the fine details of turbulence-induced distortions imprinted into the receiver modes a large number $Q \gg S$ of pixel modes [21] is employed at the receiver's end.

Singular modes of frozen turbulence.— Let us now investigate the properties of singular modes associated with an *instantaneous* atmospheric realization, i.e., in *frozen turbulence*. In this case, the distribution of singular values averaged over random realizations is known in the asymptotic regime of weak scintillation [22], and aligns with our results. However, our present numerical approach captures the properties of the singular modes under general, non-asymptotic turbulence conditions, and thus considerably expands over earlier studies [22–24]. Examples of intensity and phase distributions of highly-transmitting (i.e., associated singular values τ_s close to one) source (a) and receiver (b) singular modes are shown in Fig. 2, for three values of r_0 corresponding to weak, moderate and strong scintillation (left to right). Note that in strong turbulence, the source modes exhibit a *transverse localization* over areas with linear size comparable to the Fried parameter r_0 , the latter being small compared to the aperture's diameter, leading to reduced transverse scattering losses and, thus, large transmission [25]. Moreover, *non-trivial phases* of both, the source and

receiver modes (encoded in the color gradient in Fig. 2) are another salient feature – highlighting the relevance of constructive interference effects: We have numerically observed that even slight phase alterations of the source singular modes significantly reduce the transmitted power through the originally associated atmospheric realization.

The mean singular values versus mode numbers of 500 random realizations for different turbulence parameters are shown in Fig. 2(c). The black dash-dot curve corresponds to the case of weak scintillation, and exhibits a plateau of about 80 perfectly-transmitting singular modes with $\bar{\tau}_s = 1$, where the bar designates the random average. It is counterbalanced by a large number of modes with vanishing transmittance, i.e., with $\bar{\tau}_s = 0$, which altogether leads to a *bimodal* averaged singular value distribution, see Fig. 2(d). This sharp separation between open ($\bar{\tau}_s \sim 1$) and closed ($\bar{\tau}_s \sim 0$) channels agrees with the singular value distribution observed in the absence of [26] or in weak turbulence [22], as well as in other complex scattering systems [3, 27, 28]. However, in presence of partial channel control, the open channels evolve into partially transmitting channels ($\bar{\tau}_s < 1$) [29]. Accordingly, as shown by the dashed blue (moderate) and the red solid (strong scintillation) curves in Fig. 2(c), the open-channels plateau shrinks with increasing turbulence, and eventually turns into a monotonic decay of the transmittance for strong scintillation. In the latter regime, the resulting *unimodal* singular value distribution is dominated by lossy channels. Notwithstanding, even in this case, we identify more than ten modes with singular values $\bar{\tau}_s > 0.9$.

Stability of spatial modes in dynamic turbulence.— Given a non-negligible set of highly transmitting modes even in the limit of strong, static turbulence, we need to address their stability under the atmosphere’s dynamical evolution. To account for the latter in our modeling, we adopt *Taylor’s hypothesis* [30], which states that, at given turbulence parameters, an atmospheric state changes due to the flow of “frozen” turbulent eddies. In our model, this is tantamount of transverse shifts of individual phase screens with respect to the propagation direction, according to appropriate *velocity distributions* V [17, 31], as illustrated in Fig. 1. For simplicity, we here assume Gaussian-distributed transverse winds with mean $\langle V \rangle$ and variance ΔV^2 . The *atmospheric coherence time* then reads $t_c = 6.88^{-3/5} r_0 / \langle V \rangle$ [1].

Propagation of highly-transmitting modes $v_s(\rho)$ associated with a specific realization of frozen turbulence through such a dynamically evolving medium yields at the receiver’s end for $t > 0$ some *unknown* field $f_s(\rho', t)$ satisfying, by Eq. (2), the initial condition $f_s(\rho', 0) \equiv \sqrt{\bar{\tau}_s} u_s(\rho')$. The *transmitted power*, on average, is consequently given by $P_s(t) := \overline{\langle f_s(\rho', t), f_s(\rho', t) \rangle}$ (i.e., $P_s(0) = \bar{\tau}_s$), and the *stability* of the mode $v_s(\rho)$ can be characterized by the decay law followed by $P_s(t)$, to-

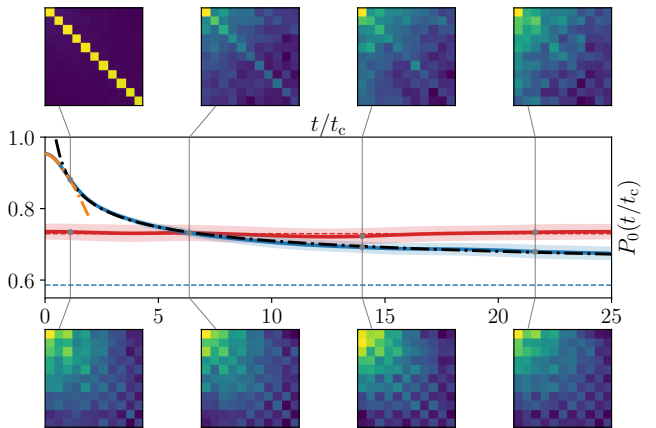


Figure 3. Mean transmitted power and crosstalk matrices [33] of highest-transmitting singular modes (blue, top) and an optimized LG modes (red, bottom) versus t/t_c in strong turbulence ($\sigma_R^2 = 6.72$, $r_0 = 15$ mm; same channel geometry as previously [21]) with $t_c = 1.57$ ms [34] (error bands give one standard deviation of 150 realizations). The singular modes’ power transmittance was identified as an initial exponential decay (orange) for $t \lesssim t_c$ saturating algebraically (black) for $t > t_c$, cf. Eq. (3). Dashed horizontals (same color coding) represent transmission through uncorrelated turbulence coinciding with the independently found asymptotic limit of the algebraic decay for singular modes.

gether with the evolution of the mean *crosstalk* matrix, $C_{s,s'}(t) := \overline{\langle f_{s'}(\rho', t), u_s(\rho') \rangle}$, which quantifies the dynamically induced, undesired transfer of amplitude from $u_s(\rho')$ into other output modes (definitions for LG modes see in footnote [32]). We benchmark this stability against that of LG modes with a waist chosen such as to maximize transmission in vacuum, and subject to ideal phase correction [9] by adaptive optics (AO), i.e., all phase errors attained by a propagated plane wave are subtracted from the received modes.

The middle row of Fig. 3 compares the transmitted power of the highest-transmitting singular mode (blue) to the AO-corrected Gaussian (i.e., LG, $p = \ell = 0$) mode (red) at strong turbulence with $\sigma_R^2 = 6.72$, as a function of time t , in units of t_c (this rescaling is convenient since it renders the temporal dynamics of $P(t/t_c)$ and $C_{s,s'}(t/t_c)$ independent of $\langle V \rangle$). It is evident that the singular mode with the largest singular value τ_0 outperforms the – in essence time independent – power transmission of the Gaussian mode for sufficiently short time scales $t < t_{\text{int}} \simeq 6 t_c$, where t_{int} denotes the time when the transmitted powers of singular modes and LG modes, both ordered by transmittance, intersect. A careful fit for the singular modes’ performance establishes the law

$$P_s(t/t_c) = \begin{cases} \bar{\tau}_s \exp[-a_s(t/t_c)^{5/3}] & t \lesssim t_c \\ b_s (t/t_c)^{-c_s} + d_s & t > t_c, \end{cases} \quad (3)$$

that is an initial *exponential* decay transitioning into a *subdiffusive* (i.e., $c_s < 1/2$) *algebraic* decay for $t > t_c$ [35].

The short time behavior is similar to the known decay law $\exp[-(t/t_c)^{5/3}]$ of the *Strehl ratio* [1], a quantifier of imaging quality in optics [8, 36]. This feature was anticipated since highly-transmitting modes and short-time images are signatures of a particular realization of turbulence. However, the subsequent algebraic decay of transmitted power for $t > t_c$ is remarkable. Its form may be attributed to long-range transverse spatial correlations of Kolmogorov turbulence (stemming from the power-law $\kappa^{-11/3}$) which translate into a long-term memory of the initial atmospheric realization. Ultimately, when all specific information of the initial configuration has faded away, the transmitted power levels off into a plateau. This lower bound of $P_s(t/t_c)$ (blue dashed line in Fig. 3) can be extracted by propagation of singular modes through uncorrelated (rather than wind-shifted, see Fig. 1) phase screens, and exactly matches the asymptotic limit $t \rightarrow \infty$, i.e., d_s in Eq. (3). The time independence of the Gaussian mode’s transmission is due to the fact that no information on the turbulent medium is inscribed into it, in contrast to the singular modes.

The relative stability of highly transmitting singular modes as suggested by the above time dependence of the transmitted power is further confirmed by comparison of the crosstalk matrices of singular versus optimized LG $p = 0$, $|\ell| \leq 5$ modes, at different times (respectively top and bottom rows of Fig. 3). While the eleven most transmitting singular modes’ $C_{s,s'}(t/t_c)$ exhibits a prominent diagonal structure – hence negligible crosstalk – for $t \leq t_{\text{int}}$ (which even leaves a fingerprint for longer times), the LG modes feature strong crosstalk at all times.

Let us finally assess the scaling of the time interval t_{int} over which singular modes transmit better than LG modes with the scintillation strength σ_R^2 . For this purpose, we compare the time dependence of the transmitted power of singular and LG ($p = 0$, $|\ell| \leq 5$) modes, ordered by their respective transmitted power fractions, and extract t_{int}/t_c . The result is shown in Fig. 4 for the two best transmitting modes, under the same conditions as in Fig. 3: t_{int}/t_c is a *nonlinear*, monotonically increasing function of the Rytov variance. This means that the advantage offered by singular modes over LG modes improves with increasing turbulence strength. The growth of t_{int}/t_c with the turbulence strength gets faster for higher order modes (compare the orange and blue curves in Fig. 4). In fact, for a fixed turbulence strength, the transmittance of the LG modes decreases quickly with increasing $|\ell|$, as reported for the first ($p = \ell = 0$; red) and second ($p = 0$, $|\ell| = 1$; green) LG mode in the insets of Fig. 4. On the contrary, all considered eleven singular modes perform similarly well (the two highest-transmitting modes are represented by respectively blue and orange curves in the insets of Fig. 4). This is consis-

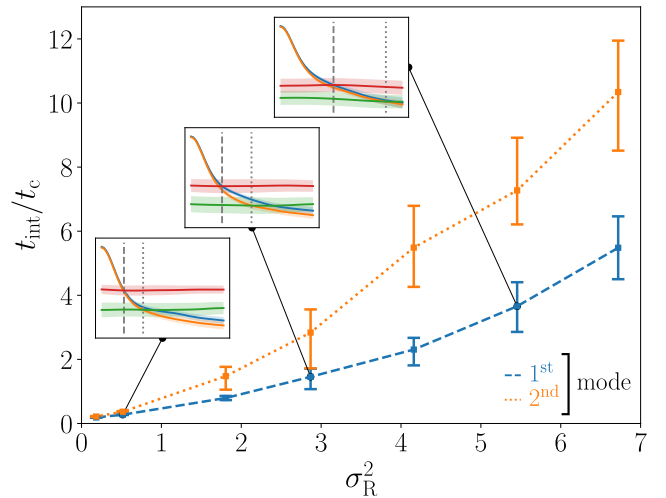


Figure 4. Rescaled average time interval t_{int}/t_c versus Rytov variance during which the highest (blue dashed) and second-highest (orange dotted) transmitting singular modes transmit more power than respective LG modes (error bars give one standard deviation of 150 realizations). The insets sketch the average transmitted power of the two highest-transmitting singular (blue, orange) and LG (red, green) modes versus rescaled time (cf. Fig. 3) with vertical lines indicating corresponding intersections.

tent with our above discussion of the distinct crosstalk properties of singular and LG modes (cf. Fig. 3). In particular, it emphasizes the potential benefit of singular modes for *multi-mode* applications in *dynamical* disordered media.

Conclusion.— This work opens new venues of future research which stem from the universality of our approach. Indeed, the split-step method and the subsequent decomposition of the transmission matrix may be applied to any channel geometry and any turbulent medium, including non-Kolmogorov models or underwater channels. It would be particularly interesting to examine whether the main features that we found, such as the slow power-law decay of transmitted power, are preserved in different dynamic disordered media. Finally, recent experimental efforts have been dedicated to the spatiotemporal characterization of disorder optical media, see e.g. the measurement of the a time-gated transmission matrix in [37]. We expect that combining these experimental advances with our theoretical characterization tools could lead to new levels of control of light transmission in time-dependent disordered optical media.

Acknowledgements.— The authors are thankful for the fruitful discussions with Szymon Gładysz. We also acknowledge financial support of the Studienstiftung des deutschen Volkes and the resources of the bwFor-Cluster. This work was partially funded by French ANR under COSMIC project (ANR-19-ASTR0020-01). V.S. and A.B. acknowledge partial funding and sup-

port through the Strategiefonds der Albert-Ludwigs-Universität Freiburg and the Georg H. Endress Stiftung.

[1] F. Roddier, *Adaptive Optics in Astronomy* (Cambridge University Press, Cambridge, 2004).

[2] G. Labeyrie, F. Tomasi, J. Bernard, C. A. Müller, C. Miniatura, and R. Kaiser, *Phys. Rev. Lett.* **83**, 5266 (1999).

[3] O. N. Dorokhov, *Solid State Commun.* **51**, 381 (1984).

[4] Michael C. Roggemann, B. M. Welsh, and R. Q. Fugate, *Rev. Mod. Phys.* **69**, 437 (1997).

[5] Y. Ren, G. Xie, H. Huang, C. Bao, Y. Yan, N. Ahmed, M. P. J. Lavery, B. I. Erkmen, S. Dolinar, M. Tur, M. A. Neifeld, M. J. Padgett, R. W. Boyd, J. H. Shapiro, and A. E. Willner, *Optics Lett.* **39**, 2845 (2014).

[6] Y. Ren, L. Li, Z. Wang, S. M. Kamali, E. Arbabi, A. Arbabi, Z. Zhao, G. Xie, Y. Cao, N. Ahmed, Y. Yan, C. Liu, A. J. Willner, S. Ashrafi, M. Tur, A. Faraon, and A. E. Willner, *Sci. Rep.* **6** (2016).

[7] J. Zhao, Y. Zhou, B. Braverman, C. Liu, K. Pang, N. K. Steinhoff, G. A. Tyler, A. E. Willner, and R. W. Boyd, *Opt. Express* **28**, 15376 (2020).

[8] R. Tyson, *Principles of adaptive optics* (CRC Press, Boca Raton, 2016).

[9] G. Sorelli, N. Leonhard, V. N. Shatokhin, C. Reinlein, and A. Buchleitner, *New J. Phys.* **21**, 023003 (2019).

[10] S. Rotter and S. Gigan, *Reviews of Modern Physics* **89** (2017).

[11] M. Segev, Y. Silberberg, and D. N. Christodoulides, *Nat. Photonics* **7**, 197 (2013).

[12] L. Andrews, *Laser beam propagation through random media* (SPIE, Bellingham, 2005).

[13] A. N. Kolmogorov, *Proc. R. Soc. Lond. A* **434**, 9 (1941).

[14] A. Ishimaru, *Wave Propagation and Scattering in Random Media* (Academic Press, New York, 1978).

[15] V. I. Tatarskii, *Wave propagation in a turbulent medium* (Dover Publications, Mineola, 2016).

[16] J. Schmidt, *Numerical simulation of optical wave propagation with examples in MATLAB* (SPIE, Bellingham, 2010).

[17] V. P. Lukin, *Adaptive beaming and imaging in the turbulent atmosphere* (SPIE, Bellingham, 2002).

[18] E. M. Johansson and D. T. Gavel, in *Amplitude and Intensity Spatial Interferometry II*, edited by J. B. Breckinridge (SPIE, 1994).

[19] N. A. Roddier, *Opt. Eng.* **29**, 1174 (1990).

[20] D. A. B. Miller, *Adv. Opt. Photonics* **11**, 679 (2019).

[21] Parameters for our free-space channel: light wavelength $\lambda = 1550$ nm, propagation distance $L = 2.5$ km, diameters of source and receiver apertures $D_s = 20$ cm and $D_r = 25$ cm, respectively. For transmitter and receiver bases we employ $S = 496$ LG modes (beam waist $w_0 = 18$ mm, radial and azimuthal indices $p, |\ell| \leq 15$) and $Q = 221^2$ pixels (respectively).

[22] J. H. Shapiro, *Appl. Opt.* **13**, 2614 (1974).

[23] J. M. Kahn and A. Belmonte, in *Broadband Access Communication Technologies XII*, edited by B. B. Dingel, K. Tsukamoto, and S. Mikroulis (SPIE, 2018).

[24] L. Borcea, J. Garnier, and K. Sølna, *J. Opt. Soc. Am. A* **37**, 720 (2020).

[25] V. N. Shatokhin, D. Bachmann, G. Sorelli, N. Treps, and A. Buchleitner, in *Environmental Effects on Light Propagation and Adaptive Systems III*, edited by K. Stein and S. Gladysz (SPIE, 2020).

[26] D. Slepian, *J. Opt. Soc. Am.* **55**, 1110 (1965).

[27] Y. V. Nazarov, *Phys. Rev. Lett.* **73**, 134 (1994).

[28] C. W. J. Beenakker, *Rev. Mod. Phys.* **69**, 731 (1997).

[29] A. Goetschy and A. D. Stone, *Phys. Rev. Lett.* **111**, 063901 (2013).

[30] G. I. Taylor, *Proc. R. Soc. Lond. A* **151**, 421 (1935).

[31] E. Anzuola and S. Gladysz, *Opt. Eng.* **56**, 1 (2017).

[32] For the definitions of transmitted power $P_s(t)$ and crosstalk $C_{s',s}(t)$ in the case of LG modes, s denotes the azimuthal index $\ell = 0, \pm 1, \dots, \pm 5$ with $f_{s'}(\rho', t)$ given by LG modes propagated through evolved turbulence at time t and $u_s(\rho')$ corresponds to LG modes propagated through vacuum.

[33] Crosstalk matrices are inset in Fig. 3 at $t/t_c = 0.95, 6.36, 14.00$ and 21.63 . x - and y - axes correspond to eleven singular (top) or $p = 0, |\ell| \leq 5$ LG (bottom) modes at $t = 0$, while horizontal axes to the transmitted modes ordered by transmittance (with modes at the bottom corrected by AO).

[34] $\langle V \rangle = 3$ m/s and $\Delta V = 1$ m/s (Gaussian distribution).

[35] Figure 3 shows $P_0(t/t_c)$ with $a_0 = 0.200$, $b_0 = 0.305$, $c_0 = 0.391$, and $d_0 = 0.586$.

[36] M. Born and E. Wolf, *Principles of optics : electromagnetic theory of propagation, interference and diffraction of light* (Cambridge University Press, Cambridge, 1999).

[37] L. Devaud, B. Rauer, M. Kühmayer, J. Melchard, M. Mounaix, S. Rotter, and S. Gigan, (2022), arXiv:2202.01597 [physics.optics].